Separation and Purification Technology 259 (2021) 118113

Contents lists available at ScienceDirect

Separation and Purification Technology

journal homepage: www.elsevier.com/locate/seppur

CO_2/H_2 separation through poly(ionic liquid)–ionic liquid membranes: The effect of multicomponent gas mixtures, temperature and gas feed pressure

Andreia S.L. Gouveia [a], María Yáñez [b], Vítor D. Alves [c], J. Palomar [d], C. Moya [d], Daniel Gorri [b], Liliana C. Tomé [e], Isabel M. Marrucho [a,*]

[a] Centro de Química Estrutural, Instituto Superior Técnico, Universidade de Lisboa, Avenida Rovisco Pais, 1049-001 Lisboa, Portugal
[b] Department of Chemical and Biomolecular Engineering, University of Cantabria, Av. Los Castros 46, 39005 Santander, Spain
[c] LEAF, Linking Landscape, Environment, Agriculture and Food, Instituto Superior de Agronomia, Universidade de Lisboa, Tapada da Ajuda, 1349-017 Lisboa, Portugal
[d] Sección de Ingeniería Química. Universidad Autónoma de Madrid, 28049 Madrid, Spain
[e] POLYMAT, University of the Basque Country UPV/EHU, Avenida Tolosa 72, Donostia-San Sebastian 20018, Gipuzkoa, Spain

ARTICLE INFO

Keywords:
Poly(ionic liquid)s
Ionic liquids
PIL–IL composites
Mixed CO_2/H_2 separation
COSMO-RS analysis

ABSTRACT

This work presents mixed gas separation performance through PIL–IL membranes bearing pyrrolidinium-based PILs with $[NTf_2]^-$ and $[C(CN)_3]^-$ anions and different weight percentages of the corresponding ILs using a ternary mixture of H_2, CO_2 and N_2 and different feed pressures ranging from 1 to 4 bar and temperatures from 20 to 80 °C. COSMO-RS was successfully used to understand the separation behavior of the PIL–IL composites for the $H_2 + CO_2 + N_2$ mixture. The effect of temperature between 20 °C and 80 °C and feed pressure between 1 bar and 4 bar was also studied and is here discussed. The increased of the mixed H_2, CO_2 and N_2 permeabilities with increasing temperature was shown to be due to dominant role of gas solubility at low temperature, and diffusivity at high temperature. The small pronounced differences between mixed and ideal CO_2/H_2 permselectivities through the prepared PIL–IL composites indicated that membrane separation efficiency can be maintained, despite the competition effect between gases in mixed gas experiments. Depending on the operating conditions, the best mixed separation performance was obtained for PIL $C(CN)_3$–60 $[C_2mim][C(CN)_3]$, with a CO_2 permeability of 324.7 Barrer and a CO_2/H_2 permselectivity of 11.4. The great potential of the studied PIL–IL membranes for biohydrogen separation is here clearly evidenced, since they revealed mixed CO_2/H_2 separation performances above the Robeson upper bound even at the highest temperature and feed pressure tested.

1. Introduction

Despite the enormous potential of hydrogen (H_2) as an energy solution, the fact that it is not a primary fuel source, since it needs to be produced or isolated prior to use [1], greatly hinders its full potential. In recent years, the promising and renewable characteristics of H_2 led to development of several biological routes to production. Biohydrogen ($bioH_2$) production is catalyzed by microorganisms in an aqueous environment, close to ambient temperature (30–35 °C) and atmospheric pressure conditions. This makes $bioH_2$ production less energy intensive and more environmentally friendly compared to conventional thermochemical and electrolysis H_2 production systems [2,3]. Additionally, biological H_2 production can use several waste materials, facilitating waste recycling [4]. Biological systems for H_2 production can be divided in two main categories: light-dependent (direct or indirect biophotolysis and photo fermentation) and -independent (dark fermentation) methods [4–7]. Despite its low hydrogen yields and production rates, the non-requirement of light energy and high rate of cell growth make dark or anaerobic fermentation, a promising cost-effective $bioH_2$ production method [4]. However, to get an enriched H_2 stream for efficient energy production, the elimination of other gases, mainly CO_2, N_2 and other impurities (H_2O and H_2S) is an important issue that needs to be solved [8].

Ionic liquids (ILs) have been shown to be a successful platform to design novel task-specific materials for gas separation due to their intrinsic properties such as negligible vapor pressure and tunable nature [9]. The simplest approach to use ILs as gas separation membranes is through supported ionic liquid membrane (SILM), in which IL is immobilized into the pores of an inert porous support [10]. In what concerns the use of IL–based membranes for gas separation, single gas

* Corresponding author.
E-mail address: isabel.marrucho@tecnico.ulisboa.pt (I.M. Marrucho).

https://doi.org/10.1016/j.seppur.2020.118113
Received 16 September 2020; Received in revised form 20 November 2020; Accepted 21 November 2020
Available online 27 November 2020
1383-5866/

permeability and ideal selectivity data are fundamental to determine the most suitable ILs for a specific gas separation. However, the gas permeation properties of one gas may be altered by the presence of other gases in a gas mixture, eventually leading to different limitations phenomena as competitive sorption, penetrant induced plasticization or concentration polarization [11–13]. In this context, several works have been evaluated the performance of IL–based membranes for the separation of gas mixtures [14–20]. For instance, mixed gas selectivities for two different gas pairs (CO_2/CH_4 and CO_2/N_2) through [C_2mim][BF_4], [C_2mim][DCA] and [C_2mim][CF_3SO_3]-based SILMs were reported by Scovazzo et al. [16], and it was observed that they are similar to the ideal gas selectivities. The reported SILMs did not reduce their separation ability even under CO_2 partial pressure of 2 bar. On the other hand, Zarca et al. [15] studied both single and mixed gas permeation through the [C_6mim][Cl]-based SILM for CO_2, H_2, CO and N_2 and found that the mixed gas permeabilities decreased compared to the single gas permeabilities. Chen et al. [17] also reported the single and mixed H_2, N_2 and CO_2 permeation through PVDF–[C_2mim][$B(CN)_4$] composites at 35 °C and 2 bar of feed pressure. In this work, the slight reduction in mixed CO_2 permeability and CO_2/N_2 and CO_2/H_2 selectivities compared to the single gas experiments was attributed to the competitive sorption in mixed gas separation systems [17]. More recently, Noble et al. demonstrated that IL-based epoxy-amine ion gel membranes can maintain or even increase their CO_2/CH_4 [19] and CO_2/N_2 [20] selectivities under humidified mixed gas streams.

Poly(ionic liquid)s (PILs) and their derived composite materials incorporating ionic liquids (PIL–IL) are a highly promising strategy to design membranes with improved CO_2 separation ability [9,21–23]. However, only a small number of studies concerning mixed gas separation performance through PIL–based membranes have been published to date. Recently, Nikolaeva et al. [24] reported the performance of PIL-based thin-film composite membranes containing the same anion ($[NTf_2]^-$) and three different polycations, namely poly(vinylbenzyl(2-hydroxyethyl)dimethylammonium (poly($[VBHEDMA]^+$)), poly(vinylbenzyltrimethylammonium) (poly($[VBTMA]^+$)) and poly(vinylbenzylmethylpyrrolidinium) (poly($[VBMP]^+$)) under mixed gas permeation conditions. The authors found that humidified feed gas enhanced membrane flux. The poly[VBHEDMA]-based membranes showed the highest mixed CO_2/N_2 selectivity, but also exhibited the lowest CO_2 permeance, due to the high affinity of CO_2 molecules for this specific polycation [24].

The present study steps forward in the evaluation of the mixed gas separation performance through the most promising PIL–IL composites comprising pyrrolidinium-based PILs with $[NTf_2]^-$ and $[C(CN)_3]^-$ anions and different weight percentages of the corresponding ILs, previously studied by us [23,25,26] under single gas permeation conditions. A specific multicomponent gas mixture of H_2, CO_2 and N_2 was selected as a simulated biohydrogen-containing mixture [27], and gas permeation measurements were performed at temperatures ranging from 20 to 80 °C and different feed pressures (1–4 bar). All the PIL–IL membranes were characterized in terms of their mechanical properties to analyze the blending effect of IL. A computational approach based on COSMO-RS method was also applied to further understand the obtained experimental mixed gas permeation results.

2. Experimental section

2.1. Materials

Poly(diallyldimethylammonium) chloride solution (average M_w 400,000 – 500,000, 20 wt% in water), acetone (99.8%), and acetonitrile (99.8%) were purchased from Sigma-Aldrich. Lithium bis(trifluoromethylsulfonyl)imide ($LiNTf_2$, 99 wt% pure) and sodium tricyanomethanide ($NaC(CN)_3$, 98 wt% pure) were provided by IoLiTec GmbH (Heilbronn, Germany). Poly([Pyr_{11}][$C(CN)_3$]) and poly([Pyr_{11}][NTf_2]) PILs were synthesized by anion metathesis reactions from the commercially available precursor, poly([Pyr_{11}][Cl]), according to previously established procedures [23,28]. The ionic liquids, 1-ethyl-3-methylimidazolium tricyanomethanide ([C_2mim][$C(CN)_3$], >98 wt% pure), 1-ethyl-3-methylimidazolium bis(trifluoromethylsulfonyl)imide ([C_2mim][NTf_2], >99 wt% pure), 1-butyl-1-methylpyrrolidinium bis(trifluoromethylsulfonyl)imide ([C_4mpyr][NTf_2], >99 wt% pure) were provided by IoLiTec GmbH. Carbon dioxide (CO_2), nitrogen (N_2), hydrogen (H_2) and helium (He) were used with no further purification.

2.2. Preparation of PIL–IL membranes

Free-standing membranes composed of the synthesized PILs and specific quantities of ILs having similar anions were prepared by solvent casting. The detailed description of the preparation of similar PIL–IL membranes can be found elsewhere [25]. The composition and experimental conditions of the casting procedure used to prepare the PIL–IL composites are listed in Table 1. All the obtained membranes were dried in a vacuum oven at 318 K until a constant weight was achieved and their thicknesses (86–122 μm) were measured using a digital micrometer (Mitutoyo, model MDE-25PJ, Kanagawa, Japan). Average thickness was calculated from six measurements taken at different locations of each PIL–IL membrane and used in the gas permeation properties calculations.

2.3. Mechanical properties

Puncture tests were performed using a TA XT Plus texture analyzer (Stable Micro Systems, UK) to evaluate the stress and elongation upon puncture of the studied PIL–IL composites. The membranes were punctured through a hole (diameter of 10 mm) with a cylindrical probe of 2 mm of diameter, at a constant speed rate of 1 mm s^{-1}. At least, four replicates for each membrane were performed and thus, the reported puncture stress and elongation upon puncture values are average results. The standard deviation was also determined for all the reported values.

The puncture stress was calculated according to the following equation:

$$\sigma = \frac{F}{A} \tag{1}$$

where σ is the puncture stress (Pa), F is the maximum force exerted by the probe (N) and A is the cross-sectional probe area (m^2). In order to obtain a better comparison of the experimental results without the influence of membrane thickness, the puncture stress values were normalized as follows:

$$\sigma_n = \frac{\sigma}{\ell} \tag{2}$$

where σ_n is the normalized puncture stress (MPa mm^{-1}) and ℓ is the membrane thickness (mm).

The elongation upon puncture was also calculated as follows [29]:

$$\text{Elongation upon puncture } (\%) = \left[\frac{\sqrt{r^2 + d^2} - r}{r}\right] \times 100 \tag{3}$$

where r is the radius of the film exposed in the cylindrical hole of the sample holder (mm) and d is the displacement of the probe from the point of contact to the point of puncture (mm).

2.4. Mixed gas permeation set-up

Mixed gas permeation properties through the prepared PIL–IL membranes were determined using an experimental set-up (Fig. 1) detailed elsewhere [30]. The composition of permeate and retentate streams was real-time analyzed by gas chromatography (Tracera GC-2010) equipped with a Barrier Ionization Discharge (BID) detector of ppb quantity level [30]. The effective membrane area was 15.6 cm^2 and

Table 1
Composition and experimental conditions of the casting procedure used to prepare the PIL–IL composite membranes.

PIL–IL membrane	Polymer (PIL)	Ionic Liquid (IL)	wt% of IL	Solvent	*T* (K)	Evaporation time (days)
PIL $C(CN)_3$–40 [C_2mim][$C(CN)_3$]	Poly([Pyr_{11}][$C(CN)_3$])	[C_2mim][$C(CN)_3$]	40	Acetonitrile	298	3
PIL $C(CN)_3$–60 [C_2mim][$C(CN)_3$]			60			
PIL NTf_2–40 [C_4mpyr][NTf_2]	Poly([Pyr_{11}][NTf_2])	[C_4mpyr][NTf_2]	40	Acetone	298	2
PIL NTf_2–60 [C_4mpyr][NTf_2]			60			
PIL NTf_2–40 [C_2mim][NTf_2]	Poly([Pyr_{11}][NTf_2])	[C_2mim][NTf_2]	40	Acetone	298	2

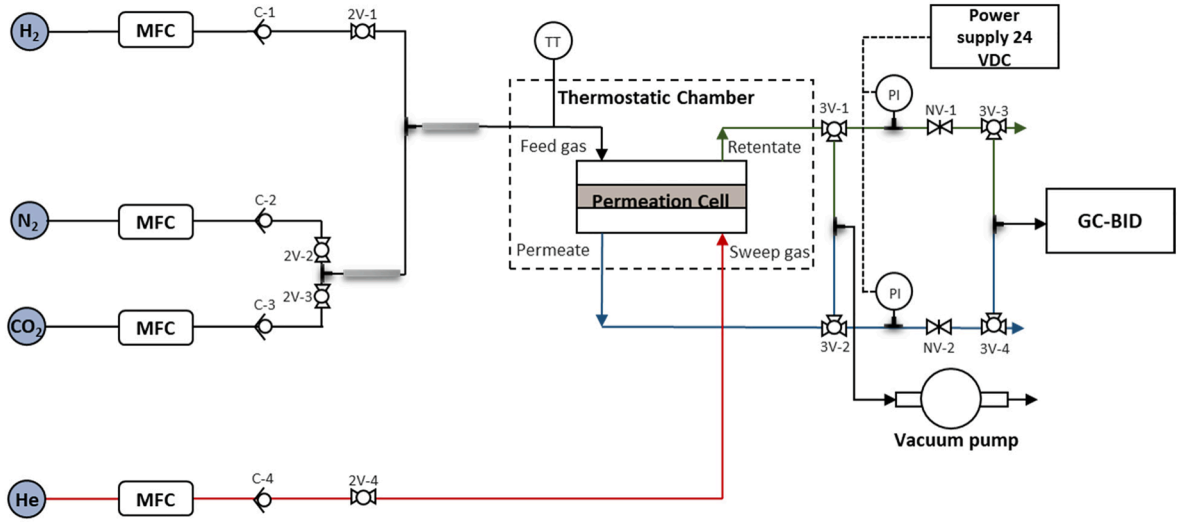

Fig. 1. Mixed gas permeation set-up. MFC, flow controller; C, check valve; 2 V, 2-way valve; 3 V, 3-way valve; TT, thermocouple; PI, pressure transducer; NV, Needle valve; GC-BID, gas analyzer. Adapted from Ref. [30].

the experiments were carried out at different temperatures (20, 35, 50, 65 and 80 °C) and at feed pressures ranging from 1 to 4 bar, with a ternary mixture of 57.1 vol% H_2, 40 vol% CO_2 and 2.9 vol% N_2. This mixture composition was chosen as an example to simulate a hydrogen-containing gas mixture produced by a biological process [27]. All the other operational parameters were kept constant: feed gas flow rate at 70 cm^3 (STP) min^{-1} and sweep gas (helium) flow rate at 20 cm^3 (STP) min^{-1}. The chosen flowrate conditions were established to guarantee that no significant concentration polarization phenomena occur in the permeate side of the membrane by setting a low stage cut (<0.5%), which is defined as the ratio of transmembrane gas flow to the feed flowrate [31]. Constant steady-state values of retentate and permeate flux and composition were reached in less than 2 h. During this period the concentration of permeate side was analyzed every nine minutes and the retentate at least five times. Once constant steady-state is reached, the gas permeability for each measurement was assessed using at least the last three injections, whose relative standard deviation for peak area was <2.1%, showing high repeatability for the gas chromatographic method used.

The experimental permeabilities of each gas were determined according to Eq. (4):

$$P = \frac{Q_{perm,T} \cdot x_{perm,i} \cdot l}{A \cdot \Delta P} = \frac{Q_{perm,T} \cdot x_{perm,i} \cdot l}{A \cdot \left(p_{feed} \cdot x_{feed,i} - p_{perm} \cdot x_{perm,i}\right)} \quad (4)$$

where $Q_{perm,T}$ is the total permeate flux through the membrane, $x_{perm,i}$ is the experimental concentration of component i in the permeate side of the membrane (vol%), l is the membrane thickness, A is the effective membrane area and ΔP is the difference in the partial pressure of the gas between both sides of the membrane. All the mixed gas permeation data reported in the results and discussion section are average values obtained from at least three experimental runs.

The mixed gas selectivity was defined as the ratio of permeability values as follows (Eq. (5)):

$$\alpha_{i/j} = \frac{P_i}{P_j} \quad (5)$$

2.5. COSMO-RS analysis

A computational approach based on COSMO-RS was applied to further understand the obtained experimental mixed gas permeation results through the PIL–IL composites. First, geometries of N_2, H_2, CO_2 and ILs were optimized at BP86/TZVP computational level, using solvent effect through COSMO method using Turbomole 7.0 software. After that, COSMOtherm program was used to compute the solubility of the different gases at the studied temperature conditions. The diffusion coefficient in ILs was estimated using a modified Wilke-Chang correlation for ILs [32].

Finally, the ideal permeability of a gas through a membrane can be calculated as the product of the diffusivity and the sorption equilibrium parameter (Henry's constant) as follows:

$$P_i = D_i \cdot K_H \quad (6)$$

where P_i is the permeability of the component i, D_i is the diffusion coefficient of the gas in the pure IL and K_H is the Henry's constant of the gas in the corresponding IL. The Henry's constant was defined in this work according to Eq. (7):

$$K_H(bar^{-1}) = \frac{x_i}{p_i} \quad (7)$$

where p_i is the partial pressure and x_i is the mole fraction of component i.

3. Results and discussion

3.1. Mechanical properties

The PIL–IL membranes were characterized in terms of their mechanical properties to analyze not only the effect of the amount of IL, but also the influence of the different IL structures. The normalized puncture stress (mPa mm^{-1}) as well as the elongation upon puncture (%) of the studied PIL–IL membranes are shown in Fig. 2 and listed in Table S1 of Supporting Information. As expected, both puncture stress and elongation upon puncture decrease with increasing the amount of IL in the composite, within the same structural family of IL. This behavior was also reported in literature by several authors and has been attributed to the plasticizing effect of IL, which reduces the membranes mechanical resistance [17,33–37].

From Fig. 2, it can be seen that the PIL NTf_2–40 $[C_2mim][NTf_2]$ membrane revealed the highest puncture stress, while the PIL NTf_2–40 $[C_4mpyr][NTf_2]$ composite showed the highest elongation upon puncture, which clearly reveals the influence of having both PIL and IL components with similar cation structure (pyrrolidinium-based cation) or having different cations in both PIL and IL structures. In fact, the presence of $[C_2mim]^+$ cation in the IL makes the corresponding PIL–IL membrane more rigid compared to $[C_4mpyr]^+$ cation, that promotes an increase of the elongation properties of the membrane. This behavior can be probably attributed to the to the chemical compatibility between the $[C_4mpyr]^+$ cation and the pyrrolidinium polycation ($[Pyr_{11}]^+$) or to a superior plasticizing effect of $[C_4mpyr][NTf_2]$ compared to $[C_2mim][NTf_2]$ IL. To evaluate the effect of anion's chemical structure, the composites containing 40 wt% of IL were used. It was observed that the membranes comprising the $[NTf_2]^-$ anion present the highest mechanical properties compared to those including the $[C(CN)_3]^-$ anion (Fig. 2), meaning that the presence of $[NTf_2]^-$ anion also promotes an increase of the elongation properties of the membrane. In fact, the following order can be established for the normalized puncture stress: PIL NTf_2–40 $[C_2mim][NTf_2]$ > PIL NTf_2–40 $[C_4mpyr][NTf_2]$ > PIL $C(CN)_3$–40 $[C_2mim][C(CN)_3]$ and for the elongation upon puncture: PIL NTf_2–40 $[C_4mpyr][NTf_2]$ > PIL NTf_2–40 $[C_2mim][NTf_2]$ > PIL $C(CN)_3$–40 $[C_2mim][C(CN)_3]$. However, for the PIL–IL composites containing 60 wt % of IL, the reverse order is obtained for both the normalized puncture stress and elongation upon puncture: PIL $C(CN)_3$–60 $[C_2mim][C(CN)_3]$ > PIL NTf_2–60 $[C_4mpyr][NTf_2]$. This reverse behavior might be due to the combined effect of both the anion and the different IL cation.

It should also be noted that although the membranes mechanical resistance decreased with increasing IL content in polymer matrix, all the prepared PIL–IL composite membranes showed adequate mechanical stability to be tested in the mixed gas permeation apparatus at the different feed pressures.

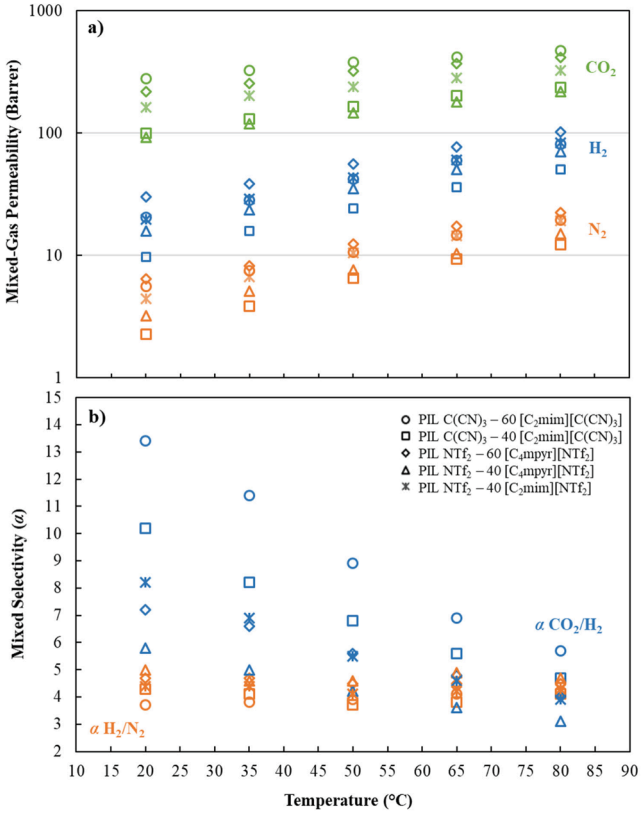

Fig. 3. Experimental mixed a) CO_2 (green), H_2 (blue) and N_2 (orange) permeabilities and b) gas permselectivities as a function of temperature at total feed pressure of 1 bar, through the PIL–IL membranes studied in this work. (For interpretation of the references to colour in this figure legend, the reader is referred to the web version of this article.)

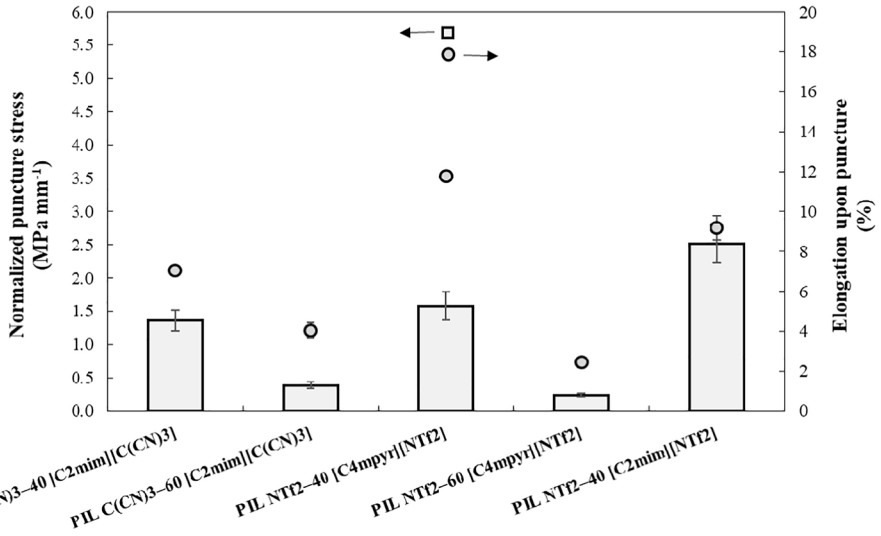

Fig. 2. Normalized puncture stress (mPa mm^{-1}) and elongation upon puncture (%) of the studied PIL–IL membranes.

3.2. Mixed gas experiments

3.2.1. Temperature effect

The effect of temperature on mixed gas permeabilities through the studied PIL–IL composite membranes (Table 1) is plotted in Fig. 3a) and listed in Table S2 of the Supporting Information. The measurements were performed at five different temperatures (20, 35, 50, 65 and 80 °C) and at a total feed pressure of 1 bar for the $CO_2 + H_2 + N_2$ gas mixture. These specific temperatures were selected considering the diverse dark fermentative H_2 production temperature conditions reported in literature, depending on the microorganism used: ambient (15–27 °C), mesophilic (30–45 °C), thermophilic (50–60 °C) and extremely thermophilic (>60 °C) [38]. The operating temperature is a key factor during fermentative process, since it can modify not only the substrate microbial use and the specific growth rate but also the bioH_2 production and metabolic product formation [38].

From Fig. 3a), it can be observed that mixed CO_2, H_2 and N_2 permeabilities increase with increasing of temperature from 20 to 80 °C. Although the H_2 composition (57.1 vol%) in the ternary mixture was higher than that of CO_2 (40 vol%) and N_2 (2.9 vol%), the same trend of gas permeabilities ($P_{CO2} > P_{H2} > P_{N2}$) was obtained for all the composites. This is in agreement to what was observed in our previous study for single gas permeabilities through similar PIL–IL membranes [25]. Moreover, enhanced mixed CO_2, H_2 and N_2 permeabilities were obtained by incorporating high amounts of IL into the membrane (Fig. 3a) and Table S2).

In order to explore the temperature dependence of the mixed gas permeability, the experimental data was correlated using an Arrhenius type equation as follows (Eq. (8)):

$$P = P_0 e^{-\frac{E_P}{RT}} \quad (8)$$

where P_0 is the pre-exponential factor (cm^3(STP) cm cm^{-2} s^{-1} $cmHg^{-1}$), E_P is the activation energy of permeation (kJ mol^{-1}), T is the temperature (K) and R is the ideal gas constant (kJ mol^{-1} K^{-1}). The E_P values were determined for each gas from the slopes of the *ln*(*P*) vs 1000/T curves and are summarized in Table 2.

The obtained correlation coefficients ($R^2 > 0.991$) for all cases, indicate the validity of the Arrhenius type dependence with temperature. The activation energy values of gas permeation through the PIL–IL composites can be ordered as follows: $CO_2 < H_2 < N_2$, except for the case of PIL C(CN)$_3$–60 [C_2mim][C(CN)$_3$], in which the activation energy of N_2 is higher compared to that of H_2. Despite this exception, the order of permeation activation energies is in agreement to what has been reported in the literature for other polymeric membranes [31,39–41]. For both PIL structures, the permeation activation energy values decrease with increasing IL content, meaning that PIL– 40 IL membranes are more sensitive to changes in temperature compared to membranes with higher amounts of IL incorporated. Overall, the high values for the activation energy of permeation for all gases show that permeability is strongly dependent on temperature.

The effect of temperature on mixed gas selectivities was also calculated and is shown in Fig. 3b) and listed in Table S2 of the Supporting Information. In the temperature range from 20 to 80 °C, the mixed CO_2/H_2 permselectivities decreased with increasing temperature, while mixed H_2/N_2 permselectivity remained approximately constant. Particularly, at bioH_2 production conditions ($T = 35$ °C and total $p_{feed} = 1$ bar), the PIL C(CN)$_3$–60 [C_2mim][C(CN)$_3$] membrane presents the highest mixed CO_2/H_2 permselectivity (11.4), while PIL NTf$_2$–40 [C_4mpyr][NTf$_2$] shows the lowest mixed CO_2/H_2 permselectivity (5.0) among all composites. Comparing these results with those of the ideal permselectivities previously reported by us [25], slightly higher CO_2/H_2 permselectivities were obtained for similar membranes ($\alpha_{CO2/H2}$ PIL C(CN)$_3$–60 [C_2mim][C(CN)$_3$] = 12.5 and $\alpha_{CO2/H2}$ PIL NTf$_2$–40 [C_4mpyr][NTf$_2$] = 4.8) under single gas permeation conditions. However, the gas permeability and CO_2/H_2 permselectivity behaviors with temperature were similar to those observed for pure gases [25]. In sum, the reduction of mixed CO_2/H_2 permselectivities at high temperatures suggests that the most favorable performances are achieved at low temperatures.

To better understand the temperature effect on mixed gas permeabilities of the studied PIL–IL membranes, the COSMO-RS method was used. Fig. S1 of the Supporting Information shows that the experimental permeabilities of pure gases (P_i^{Pure}) through similar PIL–40 IL membranes previously reported [25] present a linear relationship with the experimental mixed gas permeabilities for the $CO_2 + H_2 + N_2$ mixture ($P_i^{Mixture}$) measured in this work, at 1 bar of total feed pressure. This indicates that the permeability of these gases through PIL–IL composites behaves nearly ideal for the studied gas mixture. Thus, a theoretical model based on the properties of the pure gaseous solute + IL binary systems may be useful to understand the separation behavior of the prepared PIL–IL membranes. This can be seen in Fig. S2 of the Supporting Information, where it is shown that the gas–IL isotherms calculated using COSMO-RS in the studied range of temperature and pressure comply the Henry's law. Fig. 4 shows that, in fact, the experimental CO_2, H_2 and N_2 mixed gas permeability values through PIL–40 IL composites are generally well predicted by Eq. (6), in terms of Henry's equilibrium constant (K_H) and gas diffusivity coefficient in IL (D_i), both estimated from COSMO-RS calculations (see Table S3 of the Supporting Information). As exception, the calculated P_{CO2} values for the membrane containing the [C_2mim][C(CN)$_3$] IL strongly deviate from the general trend, but it is known that COSMO-RS method overestimates the CO_2 solubility in this IL [42]. Removing [C_2mim][C(CN)$_3$] from our analysis, the mixed experimental versus calculated permeability values through the membranes containing [C_2mim][NTf$_2$] and [C_4mpyr][NTf$_2$] ILs present a linear relationship with $R^2 > 0.96$, slope close to 1 (0.9) and intercept close to 0 (1.2 Barrer). The mean absolute error for permeability predictions is relatively low (16.3 Barrer).

Table 2
Activation energy, E_P, (kJ mol^{-1}) of gas permeation through the studied PIL–IL membranes at total $p_{feed} = 1$ bar, according to Eq. (8).

Membrane sample	E_P (kJ mol^{-1})		
	CO_2	H_2	N_2
PIL C(CN)$_3$ – 40 [C_2mim][C(CN)$_3$]	12.4	23.6	24.5
PIL C(CN)$_3$ – 60 [C_2mim][C(CN)$_3$]	7.5	20.1	18.0
PIL NTf$_2$ – 40 [C_4mpyr][NTf$_2$]	12.3	21.4	21.8
PIL NTf$_2$ – 60 [C_4mpyr][NTf$_2$]	9.6	18.0	18.6
PIL NTf$_2$ – 40 [C_2mim][NTf$_2$]	9.8	20.7	21.4

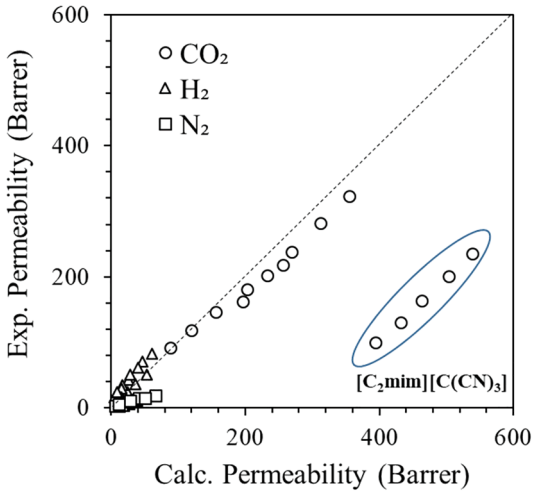

Fig. 4. Mixed experimental vs calculated (Eq. (6)) CO_2, H_2 and N_2 permeabilities through PIL–40 IL membranes, at the different studied temperatures and 1 bar of feed pressure.

In Fig. 5, an analysis of the K_H and D_i, for each gas, calculated with COSMO-RS and used in Eq. (6) to obtain pure gas permeability shown in Fig. 4, is presented. It can be concluded that the higher permeability of CO_2 in comparison to that of H_2 and N_2 is mainly due to the higher K_H values, i.e. the higher solubility of CO_2 in IL. On the other hand, the P_{H2} and P_{N2} values seem to be determined by both the gas solubility (higher for N_2) and the diffusivity (higher for H_2), in good agreement with literature [43]. It can also be observed that the general effect of increasing the permeability with increasing temperature is ascribable to the increasing of diffusivity contribution. The high temperature leads to high D_i values, due to the lower viscosity of IL [42], and implies low gas solubility, except in the case of H_2, which presents an "inverse" temperature effect, in good agreement with experimental evidences [44]. Attending to Fig. 5a, at low temperatures, the CO_2 solubility determines its permeability behavior through the composite, whereas, at 80 °C, CO_2 permeability is controlled by the diffusivity. However, in any case, the changes on both K_H and D_i values, due to the IL nature and operating temperature, do not affect the CO_2 permeability order.

Regarding the effect of IL, the COSMO-RS excess enthalpy, entropy and Gibbs free energy of gas-solvent are presented in Fig. 6. The thermodynamics of CO_2 + IL binary mixture is governed by the exothermic enthalpy (Fig. 6a), mainly determined by the establishment of attractive van der Waals interactions (Fig. 6b). The favorable entropic contribution plays a major role in the case of H_2 + IL mixture (Fig. 6a), explaining the observed "inverse" temperature effect of H_2 solubility in IL. Interesting, COSMO-RS predicts that the solubility of N_2 in IL can be decreased by promoting unfavorable electrostatic (misfit: MF) intermolecular solute–solvent interactions.

The current computational COSMO-RS analysis proved to be a very helpful tool to understand the performance of the PIL–IL membranes to separate CO_2 from H_2 and N_2 in a multicomponent gas mixture. The selection of new ILs with promising absorbent characteristics through the screening new cations and anions using COSMO-RS is a promising line of research to optimize the membrane gas separation behavior.

3.2.2. Feed pressure effect

The mixed CO_2, H_2 and N_2 permeabilities and respective permselectivities were also evaluated as a function of total feed pressure (Fig. 7a) and b) and Table S4 of the Supporting Information). The experiments were performed at $T = 35$ °C and at $p_{feed} = 1$–4 bar. It should be noted that the operating feed pressure effect on mixed gas permeability cannot be analyzed by the computational approach based on COSMO-RS method, since Eq. (6) does not depend on pressure.

From Fig. 7a), it can be observed that mixed N_2 permeability slightly decreases with increasing total feed pressure for all the studied PIL–IL membranes. As for mixed CO_2 and H_2 permeabilities, both remained approximately constant with increasing feed pressure, for the membranes containing up to 40 wt% of IL. However, for PIL NTf_2–60 [C_4mpyr][NTf_2] membrane, mixed CO_2 and H_2 permeabilities decreased by around 20% and 16%, respectively, with increasing feed pressure, while for the membrane containing 60 wt% of [C_2mim][$C(CN)_3$] IL, the reduction was approximately 13% (P_{CO2}) and 4% (P_{H2}).

A parameter that influences the mixed gas separation performance of a polymeric membrane is competitive sorption, which is related to the intrinsic material properties. In multicomponent gas mixtures, the transport behavior of one gas specie through the membrane is affected by the presence of other gas components, and thus it deviates from that of the pure gas. The competitive sorption effect between gas species can be an explanation for the reduction of gas permeability with increasing feed pressure, which is more pronounced in the case of N_2, probably due to its low content in the mixture (only 2.9 vol%). Moreover, the slight decrease of CO_2 permeability with increasing total feed pressure was specifically observed in the case of membranes containing the highest amount of IL (60 wt%), and more pronounced in the PIL NTf_2–60

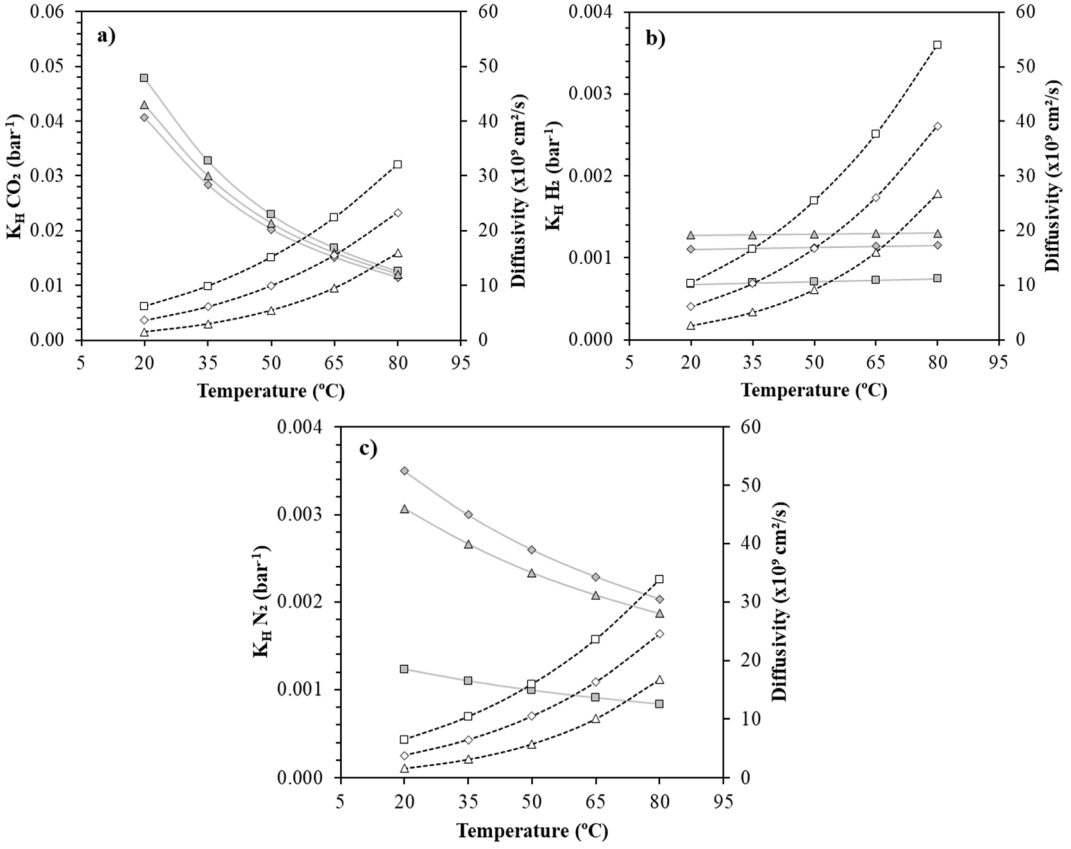

Fig. 5. Henry's equilibrium constant (K_H) (filled symbols) and gas diffusivity coefficient in IL (D_i) (white symbols) from COSMO-RS calculations used in Eq. (6). (◇) [C_2mim][NTf_2]; (□) [C_2mim][$C(CN)_3$]; (△) [C_4mpyr][NTf_2]).

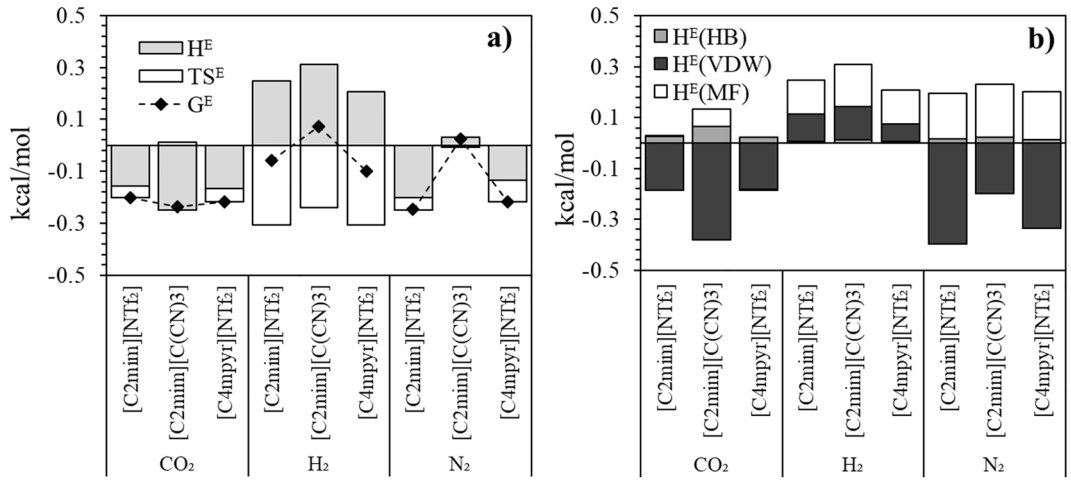

Fig. 6. a) Calculated excess properties (enthalpy, entropy and Gibbs free energy) and b) intermolecular interaction contributions [electrostatic, H^E (MF); hydrogen-bond, H^E (HB); and van der Waals, H^E (vdW)] to the excess enthalpy of equimolar mixtures of gas solute and IL computed by COSMO-RS at 20 °C.

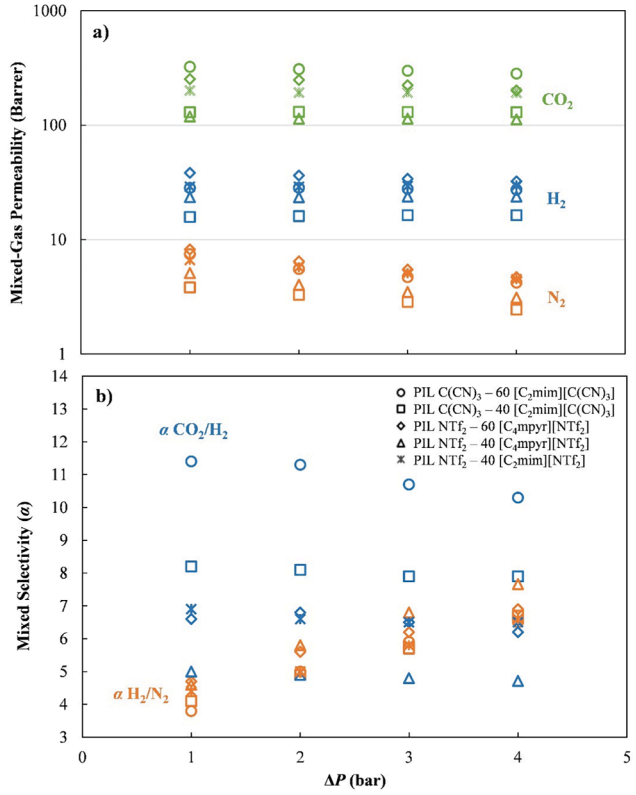

Fig. 7. Experimental mixed gas a) permeabilities and b) permselectivities as a function of total feed pressure at T = 35 °C, through the PIL–IL membranes studied in this work.

[C4mpyr][NTf_2] membrane. This behavior has been observed when CO_2 facilitated transport occurs, at low feed pressures, as reported by Shimoyama et al. [14] for SILMs containing the $[NTf_2]^-$ anion in the separation of CO_2 from a CO_2 + N_2 binary mixture, due to specific interactions of CO_2 and IL' anions comprising fluorine atoms, such as the case of $[NTf_2]^-$anion.

Fig. 7b) displays the experimental mixed gas permselectivities as a function of total feed pressure at T = 35 °C through the studied PIL–IL membranes. It can be observed that the mixed H_2/N_2 permselectivities increase with increasing feed pressure. This is probably linked to the mixed gas permeabilities behavior, where the mixed gas permeability for N_2 decreases with feed pressure, while that of H_2 remains approximately constant. In what concerns the mixed CO_2/H_2 permselectivities, they remain approximately constant with increasing total p_{feed} for all the studied composites. This can also be related to the mixed gas permeability behavior of both gases, which remain approximately constant for feed pressures between 1 and 4 bar. The PIL–IL composite membranes containing 60 wt% of IL are the only exception, in which the mixed CO_2/H_2 permselectivities slightly decrease with increasing feed pressure, for instance from 11.5 at p_{feed} = 1 bar to 10.3 at p_{feed} = 4 bar, in the case of PIL C(CN)$_3$–60 IL C(CN)$_3$.

Overall, the studied PIL–IL membranes under mixed gas conditions for CO_2/H_2 separation did not lose their separation efficiency up to p = 4 bar, since no significant changes in both mixed gas permeabilities and CO_2/H_2 selectivities were observed with increasing feed pressure.

3.3. Separation performance

3.3.1. Mixed CO_2/H_2 separation performance

The mixed CO_2/H_2 separation performances of the tested PIL–IL membranes are depicted in Fig. 8, where the CO_2/H_2 permselectivity is plotted against the permeability of the more permeable gas specie (CO_2). The upper bound developed by Rowe et al. [45] for the CO_2/H_2 gas pair at 300 K is also represented in Fig. 8. This upper bound was used to evaluate the performance of the studied PIL–IL membranes at the different temperature and total feed pressure conditions ($20 < T$ (°C) < 80; $1 < p_{feed}$ (bar) < 4).

All membranes showed mixed CO_2/H_2 separation performances above the upper bound in the whole range of temperatures and pressures studied in this work. From Fig. 8, it can be also clearly seen that mixed CO_2/H_2 separation performances of all the PIL–IL membranes are highly affected by the increase in temperature from 20 to 80 °C. As previously observed, the mixed CO_2 permeabilities through all studied membranes increase with increasing temperature, while their mixed CO_2/H_2 permselectivities decrease with increasing of temperature. However, a good balance between these two parameters was obtained at biohydrogen production temperature conditions (≈ 35 °C) in all cases.

In the case of the PIL–IL composites with less amount of IL incorporated (40 wt%), the effect of feed pressure on mixed gas permeabilities and CO_2/H_2 permselectivity is almost nonexistent, meaning that the mentioned membranes maintain their separation efficiency at the highest feed pressure tested (p_{feed} = 4 bar) and biohydrogen temperature conditions (T = 35 °C). Regarding the membranes prepared with 60 wt% of IL, the slight decrease of both mixed CO_2 permeability and CO_2/H_2 permselectivity with increasing total feed pressure is evidenced in Fig. 7. Nevertheless, the PIL C(CN)$_3$–60 IL C(CN)$_3$ composite membrane

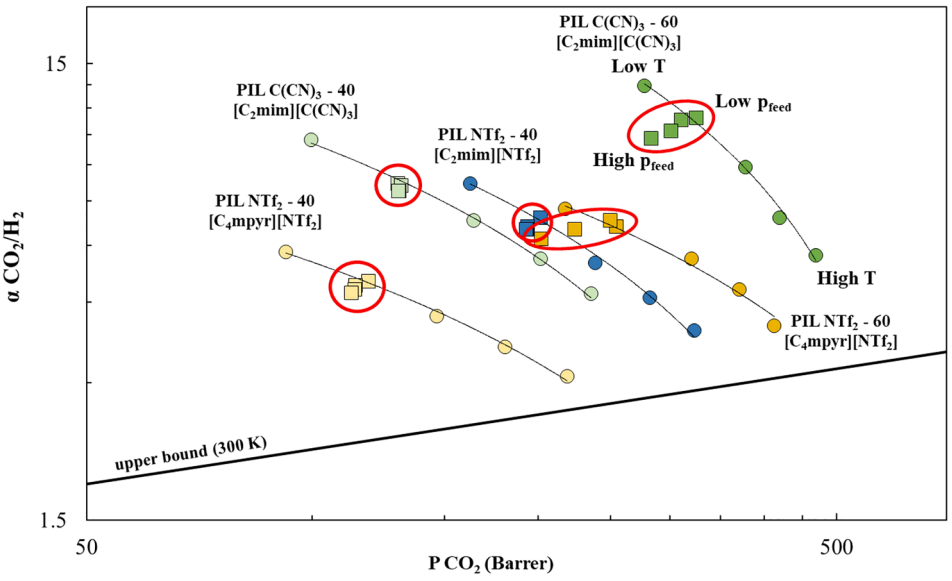

Fig. 8. Mixed CO_2/H_2 separation performance of the PIL–IL membranes studied. The experimental error is within the data points. Data are plotted on a log–log scale and the upper bound at 300 K was adapted from Rowe et al. [45]. Pressure effect on CO_2/H_2 separation performance is represented by squares and highlighted with red circles while temperature effect is represented by circles. (For interpretation of the references to colour in this figure legend, the reader is referred to the web version of this article.)

presents the best mixed CO_2/H_2 separation performances even at the highest temperature (T = 80 °C) or feed pressure (p_{feed} = 4 bar) conditions.

3.3.2. Comparison with single gas experiments

The mixed gas permeabilities as well as CO_2/H_2 permselectivities were compared to those previously reported by us for pure gases [25] through similar PIL–IL composite membranes (Table 3). In multicomponent gas mixture tests, the competitive sorption effect between CO_2, H_2 and N_2 led to a significant reduction of both CO_2 and H_2 permeabilities compared to those obtained in single gas experiments, as it can be seen from Table 3. This behavior is in agreement to what has been reported in literature for other similar gas mixtures [17,40,46,47]. Concerning the CO_2/H_2 permselectivities, the PIL C(CN)$_3$–60 IL C(CN)$_3$ membrane shows slightly lower mixed permselectivity (11.4) compared to that obtained in single gas experiments (12.2). However, the remaining composites revealed slightly higher mixed permselectivities compared to the reported ideal CO_2/H_2 permselectivities, whereas in some cases this difference is not very pronounced, leading to the conclusion that their separation efficiency can be maintained despite the competition effect between gases in mixed gas experiments.

Table 3
Mixed and single CO_2 and H_2 permeabilities (P[a]) as well as mixed and ideal CO_2/H_2 permselectivities (α) of the studied PIL–IL membranes at T = 35 °C and p_{feed} = 1 bar.[b]

Membrane sample	Mixed Gas Experiments			Single Gas Experiments[c]		
	$PCO_2 \pm \sigma$ (Barrer)	$PH_2 \pm \sigma$ (Barrer)	α CO_2/H_2	$PCO_2 \pm \sigma$ (Barrer)	$PH_2 \pm \sigma$ (Barrer)	α CO_2/H_2
PIL C(CN)$_3$–40 [C$_2$mim][C(CN)$_3$]	129.7 ± 1.4	15.7 ± 0.02	8.2	209 ± 0.9	25.9 ± 0.1	8.1
PIL C(CN)$_3$–60 [C$_2$mim][C(CN)$_3$]	324.7 ± 4.2	28.3 ± 0.03	11.4	505 ± 0.3	41.3 ± 0.8	12.2
PIL NTf$_2$ – 40 [C$_2$mim][NTf$_2$]	201.6 ± 1.0	29.0 ± 0.09	6.9	287 ± 2.4	43.9 ± 0.1	6.5
PIL NTf$_2$ – 40 [C$_4$mpyr][NTf$_2$]	118.9 ± 0.4	23.6 ± 0.03	5.0	164 ± 1.6	34.2 ± 0.3	4.8
PIL NTf$_2$ – 60 [C$_4$mpyr][NTf$_2$]	254.2 ± 1.2	38.3 ± 0.05	6.6	288 ± 1.6	45.8 ± 0.1	6.3

[a] Barrer (1 Barrer = 10^{-10} cm(STP)^3·cm·cm^{-2}·s^{-1}·cm·Hg^{-1}).
[b] The listed uncertainties represent the standard deviations (σ) based on three experiments.
[c] The single gas experiments were performed using a time-lag equipment and were taken from Gouveia et al. [25].

4. Conclusions

The mixed gas separation performance through PIL–IL membranes bearing pyrrolidinium-based PILs with $[NTf_2]^-$ and $[C(CN)_3]^-$ anions and different weight percentages of the corresponding ILs was measured in this study. Multicomponent gas mixture tests were performed using a ternary mixture of H_2, CO_2 and N_2 and different feed pressures ranging from 1 to 4 bar and temperatures from 20 to 80 °C. The mechanical properties of the selected PIL–IL membranes were assessed using puncture tests and all PIL–IL composites showed sufficient mechanical stability to be tested in the mixed gas permeation equipment at the different feed pressures, although their mechanical resistance under puncture tests decrease with increasing IL content in polymer matrix. A computational approach based on COSMO-RS method was applied to further understand the experimental mixed gas permeation results. Overall, COSMO-RS predictions revealed that the higher permeability of CO_2 compared to H_2 and N_2 is mainly due to the higher solubility of CO_2 in the IL, while H_2 and N_2 permeabilities seem to be determined by both gas solubility (higher for N_2) and diffusivity (higher for H_2) effects. From multicomponent gas mixture tests, the membranes showed mixed CO_2/H_2 separation performances above the upper bound, in the whole range of temperatures and pressures tested. Also, no significant changes in both mixed gas permeabilities and CO_2/H_2 permselectivities were observed with increasing feed pressure, meaning that the prepared composites did not lose their separation efficiency up to p = 4 bar. The competitive sorption effect between CO_2 and H_2 in mixed gas experiments led to a significant reduction in gas permeabilities compared to single gas measurements. However, CO_2/H_2 permselectivities remained practically unchanged, meaning that the separation efficiency of the studied membranes can be maintained. The PIL C(CN)$_3$–60 IL C(CN)$_3$ membrane revealed the best mixed CO_2/H_2 separation performance, even at the highest temperature (T = 80 °C) or feed pressure (p_{feed} = 4 bar) conditions.

CRediT authorship contribution statement

Andreia S.L. Gouveia: Investigation, Methodology, Writing - original draft, Writing - review & editing. **María Yáñez:** Investigation. **Vítor D. Alves:** Resources, Writing - review & editing, Supervision. **J. Palomar:** Formal analysis, Writing - review & editing. **C. Moya:** Formal analysis. **Daniel Gorri:** Conceptualization, Resources, Writing - review & editing. **Liliana C. Tomé:** Conceptualization, Writing - review & editing. **Isabel M. Marrucho:** Conceptualization, Resources, Writing - review & editing, Supervision.

Declaration of Competing Interest

The authors declare that they have no known competing financial interests or personal relationships that could have appeared to influence the work reported in this paper.

Acknowledgements

Andreia S. L. Gouveia is grateful to FCT (Fundação para a Ciência e a Tecnologia) for her Doctoral (SFRH/BD/116600/2016) research grant. Liliana C. Tomé has received funding from the European Union's Horizon 2020 research and innovation programme under the Marie Sklodowska-Curie grant agreement No 745734. Centro de Química Estrutural and Instituto Superior de Agronomia acknowledge the financial support of Fundação para a Ciência e Tecnologia (UIDB/00100/2020 and UID/AGR/04129/2020, respectively). Financial support from the Spanish AEI under projects CTQ2016-75158-R and PID2019-104369RB-I00 (AEI/FEDER, UE) is gratefully acknowledged.

Appendix A. Supplementary data

Supplementary data to this article can be found online at https://doi.org/10.1016/j.seppur.2020.118113.

References

[1] C. Casado Coterillo, B. Zornoza, A. Navajas, Chapter 11. Advances in Hydrogen Separation and Purification with Membrane Technology, in, 2013, pp. 245–268.
[2] D. Das, T.N. Veziroğlu, Hydrogen production by biological processes: a survey of literature, Int. J. Hydrogen Energy 26 (2001) 13–28.
[3] S. Meher Kotay, D. Das, Biohydrogen as a renewable energy resource—Prospects and potentials, Int. J. Hydrogen Energy 33 (2008) 258–263.
[4] L. Singh, Z.A. Wahid, Methods for enhancing bio-hydrogen production from biological process: A review, J. Ind. Eng. Chem. 21 (2015) 70–80.
[5] H.J. Alves, C. Bley Junior, R.R. Niklevicz, E.P. Frigo, M.S. Frigo, C.H. Coimbra-Araújo, Overview of hydrogen production technologies from biogas and the applications in fuel cells, Int. J. Hydrogen Energy 38 (2013) 5215–5225.
[6] D. Das, T.N. Veziroglu, Advances in biological hydrogen production processes, Int. J. Hydrogen Energy 33 (2008) 6046–6057.
[7] S. Manish, R. Banerjee, Comparison of biohydrogen production processes, Int. J. Hydrogen Energy 33 (2008) 279–286.
[8] T.C. Merkel, M. Zhou, R.W. Baker, Carbon dioxide capture with membranes at an IGCC power plant, J. Membr. Sci. 389 (2012) 441–450.
[9] L.C. Tomé, I.M. Marrucho, Ionic liquid-based materials: a platform to design engineered CO2 separation membranes, Chem. Soc. Rev. 45 (2016) 2785–2824.
[10] P. Scovazzo, Determination of the upper limits, benchmarks, and critical properties for gas separations using stabilized room temperature ionic liquid membranes (SILMs) for the purpose of guiding future research, J. Membr. Sci. 343 (2009) 199–211.
[11] S.R. Reijerkerk, K. Nijmeijer, C.P. Ribeiro, B.D. Freeman, M. Wessling, On the effects of plasticization in CO2/light gas separation using polymeric solubility selective membranes, J. Membr. Sci. 367 (2011) 33–44.
[12] G.Q. Chen, C.A. Scholes, G.G. Qiao, S.E. Kentish, Water vapor permeation in polyimide membranes, J. Membr. Sci. 379 (2011) 479–487.
[13] P. Bakonyi, N. Nemestóthy, K. Bélafi-Bakó, Biohydrogen purification by membranes: An overview on the operational conditions affecting the performance of non-porous, polymeric and ionic liquid based gas separation membranes, Int. J. Hydrogen Energy 38 (2013) 9673–9687.
[14] P. Jindaratsamee, A. Ito, S. Komuro, Y. Shimoyama, Separation of CO2 from the CO2/N2 mixed gas through ionic liquid membranes at the high feed concentration, J. Membr. Sci., s 423–424 (2012) 27–32.
[15] G. Zarca, I. Ortiz, A. Urtiaga, Behaviour of 1-hexyl-3-methylimidazolium chloride-supported ionic liquid membranes in the permeation of CO 2, H 2, CO and N 2 single and mixed gases, Desalin. Water Treat. 56 (2014) 1–7.
[16] P. Scovazzo, D. Havard, M. McShea, S. Mixon, D. Morgan, Long-term, continuous mixed-gas dry fed CO2/CH4 and CO2/N2 separation performance and selectivities for room temperature ionic liquid membranes, J. Membr. Sci. 327 (2009) 41–48.
[17] H.Z. Chen, P. Li, T.-S. Chung, PVDF/ionic liquid polymer blends with superior separation performance for removing CO2 from hydrogen and flue gas, Int. J. Hydrogen Energy 37 (2012) 11796–11804.
[18] P. Li, D.R. Paul, T.-S. Chung, High performance membranes based on ionic liquid polymers for CO2 separation from the flue gas, Green Chem. 14 (2012) 1052–1063.
[19] K. Friess, M. Lanč, K. Pilnáček, V. Fíla, O. Vopička, Z. Sedláková, M.G. Cowan, W. M. McDanel, R.D. Noble, D.L. Gin, P. Izak, CO2/CH4 separation performance of ionic-liquid-based epoxy-amine ion gel membranes under mixed feed conditions relevant to biogas processing, J. Membr. Sci. 528 (2017) 64–71.
[20] W.M. McDanel, M.G. Cowan, N.O. Chisholm, D.L. Gin, R.D. Noble, Fixed-site-carrier facilitated transport of carbon dioxide through ionic-liquid-based epoxy-amine ion gel membranes, J. Membr. Sci. 492 (2015) 303–311.
[21] J. Bara, E. Hatakeyama, D.L. Gin, R.D. Noble, Improving CO2 permeability in polymerized room-temperature ionic liquid gas separation membranes through the formation of a solid composite with a room-temperature ionic liquid, Polym. Advan. Technol. 19 (2008) 1415–1420.
[22] L.C. Tomé, A.S.L. Gouveia, C.S.R. Freire, D. Mecerreyes, I.M. Marrucho, Polymeric ionic liquid-based membranes: Influence of polycation variation on gas transport and CO2 selectivity properties, J. Membr. Sci. 486 (2015) 40–48.
[23] L.C. Tomé, M. Isik, C.S.R. Freire, D. Mecerreyes, I.M. Marrucho, Novel pyrrolidinium-based polymeric ionic liquids with cyano counter-anions: High performance membrane materials for post-combustion CO2 separation, J. Membr. Sci. 483 (2015) 155–165.
[24] D. Nikolaeva, I. Azcune, E. Sheridan, M. Sandru, A. Genua, M. Tanczyk, M. Jaschik, K. Warmuzinski, J.C. Jansen, I.F.J. Vankelecom, Poly(vinylbenzyl chloride)-based poly(ionic liquids) as membranes for CO2 capture from flue gas, J. Mater. Chem. A 5 (2017) 19808–19818.
[25] A.S.L. Gouveia, L. Ventaja, L.C. Tomé, I.M. Marrucho, Towards Biohydrogen Separation Using Poly(Ionic Liquid)/Ionic Liquid Composite Membranes, Membranes 8 (2018) 124.
[26] L.C. Tomé, D. Mecerreyes, C.S.R. Freire, L.P.N. Rebelo, I.M. Marrucho, Pyrrolidinium-based polymeric ionic liquid materials: New perspectives for CO2 separation membranes, J. Membr. Sci. 428 (2013) 260–266.
[27] M.G. Shalygin, S.M. Abramov, A.I. Netrusov, V.V. Teplyakov, Membrane recovery of hydrogen from gaseous mixtures of biogenic and technogenic origin, Int. J. Hydrogen Energy 40 (2015) 3438–3451.
[28] A.-L. Pont, R. Marcilla, I. De Meatza, H. Grande, D. Mecerreyes, Pyrrolidinium-based polymeric ionic liquids as mechanically and electrochemically stable polymer electrolytes, J. Power Sources 188 (2009) 558–563.
[29] G.W. Radebaugh, J.L. Murtha, T.N. Julian, J.N. Bondi, Methods for evaluating the puncture and shear properties of pharmaceutical polymeric films, Int. J. Pharm. 45 (1988) 39–46.
[30] M. Yáñez, A. Ortiz, D. Gorri, I. Ortiz, Comparative performance of commercial polymeric membranes in the recovery of industrial hydrogen waste gas streams, Int. J. Hydrogen Energy, (2020).
[31] T.C. Merkel, R.P. Gupta, B.S. Turk, B.D. Freeman, Mixed-gas permeation of syngas components in poly(dimethylsiloxane) and poly(1-trimethylsilyl-1-propyne) at elevated temperatures, J. Membr. Sci. 191 (2001) 85–94.
[32] C. Moya, J. Palomar, M. Gonzalez-Miquel, J. Bedia, F. Rodriguez, Diffusion Coefficients of CO2 in Ionic Liquids Estimated by Gravimetry, Ind. Eng. Chem. Res. 53 (2014) 13782–13789.
[33] M. Fallanza, A. Ortiz, D. Gorri, I. Ortiz, Polymer–ionic liquid composite membranes for propane/propylene separation by facilitated transport, J. Membr. Sci. 444 (2013) 164–172.
[34] H. Rabiee, A. Ghadimi, T. Mohammadi, Gas transport properties of reverse-selective poly(ether-b-amide6)/[Emim][BF4] gel membranes for CO2/light gases separation, J. Membr. Sci. 476 (2015) 286–302.
[35] J.C. Jansen, G. Clarizia, P. Bernardo, F. Bazzarelli, K. Friess, A. Randová, J. Schauer, D. Kubicka, M. Kacirková, P. Izak, Gas transport properties and pervaporation performance of fluoropolymer gel membranes based on pure and mixed ionic liquids, Sep. Purif. Technol. 109 (2013) 87–97.
[36] K. Friess, J.C. Jansen, F. Bazzarelli, P. Izák, V. Jarmarová, M. Kačírková, J. Schauer, G. Clarizia, P. Bernardo, High ionic liquid content polymeric gel membranes: Correlation of membrane structure with gas and vapour transport properties, J. Membr. Sci. 415–416 (2012) 801–809.
[37] H. Mannan, D. Mohshim, H. Mukhtar, M. Thanapalan, Z. Man, M. Bustam, Synthesis, characterization, and CO 2 separation performance of polyether sulfone/[EMIM][Tf 2 N] ionic liquid-polymeric membranes (ILPMs), J. Ind. Eng. Chem. 54 (2017).
[38] K. Chandrasekhar, Y.-J. Lee, D.-W. Lee, Biohydrogen Production: Strategies to Improve Process Efficiency through Microbial Routes, Int. J. Mol. Sci. 16 (2015).
[39] L. El-Azzami, E. Grulke, Dual mode model for mixed gas permeation of CO2, H2, and N2 through a dry chitosan membrane, J. Polym. Sci., Part B: Polym. Phys. 45 (2007) 2620–2631.
[40] O.C. David, D. Gorri, A. Urtiaga, I. Ortiz, Mixed gas separation study for the hydrogen recovery from H2/CO/N2/CO2 post combustion mixtures using a Matrimid membrane, J. Membr. Sci. 378 (2011) 359–368.
[41] W. Fam, J. Mansouri, H. Li, V. Chen, Improving CO2 separation performance of thin film composite hollow fiber with Pebax®1657/ionic liquid gel membranes, J. Membr. Sci. 537 (2017) 54–68.
[42] J. Palomar, M. Larriba, J. Lemus, D. Moreno, R. Santiago, C. Moya, J. de Riva, G. Pedrosa, Demonstrating the key role of kinetics over thermodynamics in the

selection of ionic liquids for CO2 physical absorption, Sep. Purif. Technol. 213 (2019) 578–586.
[43] Z. Lei, C. Dai, B. Chen, Gas Solubility in Ionic Liquids, Chem. Rev. 114 (2014) 1289–1326.
[44] S. Raeissi, C.J. Peters, Understanding temperature dependency of hydrogen solubility in ionic liquids, including experimental data in [bmim][Tf2N], AIChE J. 58 (2012) 3553–3559.
[45] B.W. Rowe, L.M. Robeson, B.D. Freeman, D.R. Paul, Influence of temperature on the upper bound: Theoretical considerations and comparison with experimental results, J. Membr. Sci. 360 (2010) 58–69.
[46] A. Farjoo, S.M. Kuznicki, M. Sadrzadeh, Hydrogen Separation by Natural Zeolite Composite Membranes: Single and Multicomponent Gas Transport, Materials 10 (2017).
[47] R.T. Chern, W.J. Koros, E.S. Sanders, R. Yui, "Second component" effects in sorption and permeation of gases in glassy polymers, J. Membr. Sci. 15 (1983) 157–169.